유연인쇄전자학술지, 2023년 0월, 제0권 제0호, 00-00
Journal of Flexible & Printed Electronics, Month 2023, Vol. 0, Issue 0
Received 2023-00-00, Revised 2023-00-00, Accepted 2023-00-00
https://doi.org/10.56767/jfpe.2022.0.0.00

RESEARCH

Localized Black Polyimide Absorbers for Low-Reflectance Ag Metal Mesh Electrodes

Ji-Sub Park[1,2], Jun-Young Jeon[1,2], Hak-Rin Kim[1,2,3*], Jun-Chan Choi[4*]

[1]School of Electronic and Electrical Engineering, Kyungpook National University, Daegu 41566, Republic of Korea

[2]XR Display Industry-Academia Research Institute, Kyungpook National University, Daegu 41566, Republic of Korea

[3]School of Electronics Engineering, Kyungpook National University, Daegu 41566, Republic of Korea

[4]School of Electrical Engineering, Pukyong National University, Busan 48513, Republic of Korea

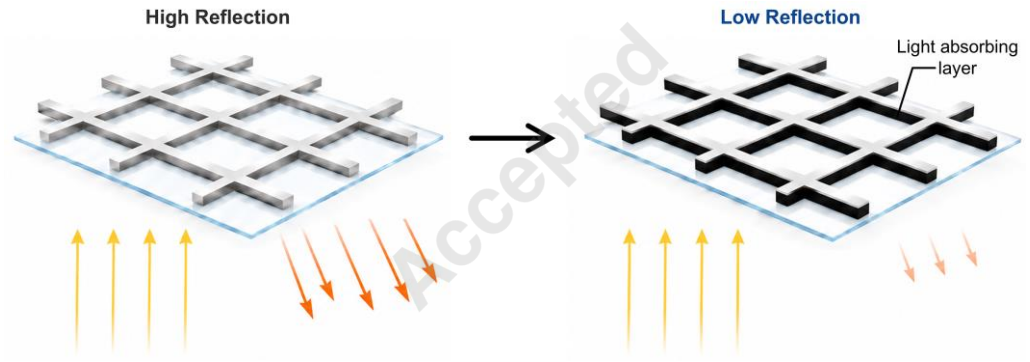

ABSTRACT

Flexible transparent conducting electrodes based on metal mesh structures can achieve low sheet resistance but often exhibit visible reflection from the metallic lines. Here, we introduce a localized black polyimide (BPI) light absorption layer near the Ag mesh lines to reduce metal-induced reflection while preserving the essential electrode characteristics. The BPI layer, consisting of carbon-black-dispersed polyimide, was patterned by combining thermal imprinting with Ag nanoparticle ink filling, thermal treatment, and selective etching, thereby localizing the light-absorption layer near the Ag mesh lines. At 550 nm, the localized BPI layer reduced the reflectance of the Ag electrode region from 50.22% to 4.94%, corresponding to a 90.16% reduction. Because the BPI layer was selectively self-positioned at the reflective metal-line region, this local reduction in reflectance provides a structural route to reducing the visibility of metal mesh electrodes. The fabricated electrode maintained transparent-electrode characteristics, with only a limited change in sheet resistance after selective etching and repeated bending.

Key Words: Transparent electrode, Metal mesh, Light absorption layer, Flexible electronics

*Correspondence: rineey@knu.ac.kr, jcchoi@pknu.ac.kr

1. INTRODUCTION

With advances in information technology, electronic devices have become increasingly integrated into nearly all aspects of daily life, driving the evolution of device form factors toward more flexible configurations [1–4]. In addition, with the growing prominence of physical artificial intelligence, the development of intelligent electronic devices capable of stable operation under dynamic conditions has accelerated, thereby increasing the demand for devices that can maintain reliable performance under mechanical deformation [5–8]. In this regard, flexible transparent conducting electrodes (TCEs) play an important role in optoelectronic devices, displays, and sensors, where they are required to maintain optical transmittance and low sheet resistance under mechanical deformation [9,10]. Although conventional indium tin oxide (ITO) electrodes offer high optical transmittance and low sheet resistance, their inherent brittleness limits their use in flexible devices [11,12]. Therefore, research efforts have been directed toward the development of alternative materials and structural designs for flexible TCEs.

Material-based approaches, including conductive polymers, metal nanowires, graphene, and carbon nanotubes (CNTs), have been proposed; however, their performance as TCEs is limited by low electrical conductivity, high junction resistance, and poor network connectivity [13–15]. As an alternative strategy, structure-based designs that address the trade-off between optical transmittance and electrical conduction have been explored. For instance, ultrathin metal configurations can improve optical transmittance, but strong optical absorption and discontinuous growth behavior limit achievable transparency [16,17]. Alternatively, patterning metals into open structures, particularly metal mesh configurations, has attracted attention as an effective approach to enhance transmittance while maintaining low sheet resistance [18–20]. However, due to the inherently high reflectivity of metals, metal mesh-based TCEs suffer from reduced visibility in bright environments and the noticeable appearance of electrode patterns. This issue arises mainly from reflection at the metallic line region, whereas the surrounding open areas are intended to maintain optical transparency. Therefore, an effective reflection-reduction strategy should target the metal-line region selectively, without covering the transparent area or altering the conductive metal network.

In this study, we introduce a flexible metal mesh TCE incorporating a localized black polyimide (BPI) light absorption layer to reduce metal-induced reflection. The BPI layer, consisting of carbon-black-dispersed polyimide, was patterned via thermal imprinting, Ag nanoparticle (NP) ink filling, thermal treatment, and selective etching, thereby self-localizing the light-absorption layer beneath and near the Ag mesh lines. This structure was designed to lower the apparent reflectance of the reflective metal-line region while preserving the essential electrical and optical characteristics required for transparent electrodes. The reflectance reduction was evaluated from the Ag electrode region, where metal-induced reflection primarily occurs. In addition, the sheet resistance and optical transmittance of the fabricated electrode were examined to assess the feasibility of localized BPI integration as a route toward low-reflectance flexible metal mesh electrodes.

2. METHODS

2.1. Materials

Ag NP-based ink was selected for the fabrication of metal mesh electrodes due to its oxidation stability and electrical conductivity [21]. To enable application on flexible film substrates via low-temperature sintering, the particle size was kept below 200 nm, and polygonal NPs were employed to increase interparticle contact area, thereby improving electrical conductivity. The Ag NP ink had an average particle size of 150 nm, a metal content of 78 ± 2 wt%, and a viscosity of 3,317 cps based on an epoxy binder, yielding resistivities of 1.78×10^{-3} and 3.84×10^{-5} Ω·cm after sintering at 150 °C and 180 °C for 30 min, respectively. Polyethylene naphthalate (PEN) film (Teonex, Teijin Dupont) was used as a flexible substrate due to its mechanical and thermal stability, showing no heat shrinkage up to 180 °C. A composite solution of polyimide (PI; 6514L, Nissan Chemical Industries, Ltd) and carbon black nanoparticles (~20 nm, 1–3 wt%) was prepared as the light absorption layer, hereafter referred to as BPI, providing suitability

for imprinting and selective etching using a potassium-based alkaline developer (potassium hydroxide:H_2O = 1:4) after soft curing [22].

2.2. Fabrication of Metal Mesh Electrodes

The fabrication process of metal mesh electrodes incorporating a light-absorption layer is illustrated in Fig. 1. A mesh-patterned polydimethylsiloxane (PDMS) stamp with protruding features was prepared by curing a PDMS mixture (base-to-curing agent ratio of 10:1) at 90 °C for 2 h. The BPI solution was bar-coated onto the PEN substrate to form a layer approximately 1.2 μm thick. The coated layer was then imprinted using the PDMS stamp at 1 kgf and thermally treated at 140 °C for 20 min to achieve soft curing, resulting in an inverse mesh structure with recessed regions corresponding to the mesh pattern. Subsequently, Ag NP ink was filled into the recessed regions using an acetal doctor blade with a 30° bevel angle, following ultraviolet–ozone (UVO) treatment for 30 min to modify the surface energy of the BPI layer and ensure uniform ink filling. After filling, the sample was thermally treated at 180 °C for 30 min to sinter the Ag electrode while simultaneously inducing selective thermal curing of the BPI in the vicinity of the electrode. Finally, the sample was immersed in an etchant solution at 80 °C for 30 s to remove the BPI layer, leaving only the regions beneath and in immediate contact with the Ag mesh electrodes, thereby forming a metal mesh electrode integrated with a light absorption layer.

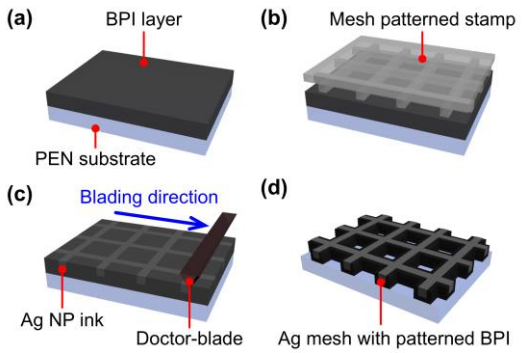

Fig. 1. Fabrication process of Ag metal mesh electrodes with a patterned BPI light absorption layer. (a) Bar-coated BPI layer on a PEN substrate. (b) Thermal imprinting of recessed mesh channels using a mesh-patterned PDMS stamp. (c) Doctor-blade filling of Ag NP ink after UVO treatment; the arrow indicates the blading direction. (d) Ag metal mesh electrode with patterned BPI after thermal treatment and selective etching.

3. RESULTS AND DISCUSSION

3.1. Design of Metal Mesh Geometry

To maintain the optical–electrical characteristics of a transparent electrode film while reducing metal-induced reflection, the metal mesh structure was designed to target a mesh sheet resistance ($R_{s,mesh}$) below 50 Ω/□ and an open-area transmittance above 95%, excluding the substrate contribution. Assuming opaque metal lines and lossless open regions, the total transmittance (T_{total}) can be approximated as $T_{total} \approx T_{substrate} \times \tau^2$, where $T_{substrate}$ is the substrate transmittance and $\tau = s/p$ is defined by the spacing s between adjacent Ag grid lines and the pattern period p [23]. Here, $p = w + s$, with w being the line width, and τ^2 represents the open area fraction of the mesh structure (Fig. 2a). Based on this relation, a line width of 5 μm and a spacing of 500 μm were selected to obtain $\tau^2 \approx 0.98$, compensating for optical losses from the PEN substrate. For the electrical design, the sheet resistance of the mesh structure was estimated using $R_{s,mesh} \approx \rho/[t(1 - \tau)]$ [23], where ρ is the resistivity obtained after thermal treatment at 180 °C for 30 min (3.84×10^{-5} Ω·cm), and t is the mesh depth. Accordingly, the mesh depth was set to approximately 1 μm to satisfy the target $R_{s,mesh} < 50$ Ω/□.

3.2. Formation of BPI-Integrated Metal Mesh Electrodes

The formation of BPI-integrated metal mesh electrodes was examined through optical microscopy (OM; LV100POL, Nikon) at representative stages of imprinting, Ag NP ink filling, and selective etching, as shown in Fig. 2b–d. After imprinting, the BPI layer showed a recessed mesh pattern transferred from the protruding PDMS stamp, with a line width of approximately 4.8 μm and a depth of approximately 900 nm (Fig. 2b,c). A residual BPI layer of about 200 nm remained between the recessed channel and the PEN substrate, placing the light absorption layer at the bottom of the channel where the metal mesh would subsequently be formed. After UVO treatment,

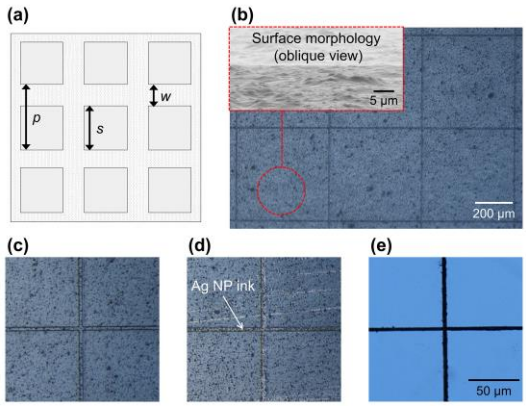

Fig. 2. Geometrical design and pattern formation of BPI-integrated Ag metal mesh electrodes. (a) Mesh design parameters. (b,c) Imprinted BPI mesh pattern; inset in (b): oblique-view scanning electron microscopy image. (d) Ag NP ink-filled mesh pattern. (e) Ag mesh pattern after thermal treatment and selective etching. OM images in (b–d) were obtained in reflection mode, whereas (e) was obtained in transmission mode.

the Ag NP ink was filled into the recessed channels by doctor blading, and the ink was largely confined within the patterned regions with only minor residue on the surrounding BPI surface (Fig. 2d). This filling behavior indicates that the surface modification of BPI helped guide the Ag NP ink into the recessed mesh channels. During the subsequent thermal treatment, the Ag NP-filled lines were sintered, while the BPI in contact with the metal mesh region underwent additional curing, thereby allowing this region to withstand the subsequent etching process. After selective etching, the optical image showed a clean metal mesh pattern with the exposed BPI regions removed (Fig. 2e), demonstrating that the sequential imprinting, filling, curing, and etching steps produced a metal mesh electrode integrated with a localized BPI light absorption layer.

3.3. Reflectance Reduction by BPI Light Absorption

The reflectance reduction effect of the BPI light-absorption layer was evaluated by measuring the local reflectance in the Ag electrode region, where metal-induced reflection primarily occurs, using a UV–vis spectrophotometer (V-650, JASCO). At 550 nm, near the wavelength range of maximum human visual sensitivity, the Ag NP ink exhibited a reflectance of 50.22%, indicating the high apparent reflectance of the metallic electrode region. When a 200 nm-thick BPI layer was introduced beneath the Ag electrode region, the reflectance decreased to 4.94%, corresponding to a reduction of approximately 90.16% (Fig. 3). This result shows that the BPI layer absorbs reflected light from the metal region and substantially lowers the apparent reflectance of the Ag electrode. Although Ag lines occupy only a small fraction of the total area in the metal mesh electrode, they are a major source of metal-induced reflection and electrode-pattern visibility. Therefore, localizing the BPI layer beneath and near the Ag mesh lines can be considered an effective structural approach for reducing reflection from the visually dominant metal-line region without introducing a light-absorbing layer over the entire transparent area.

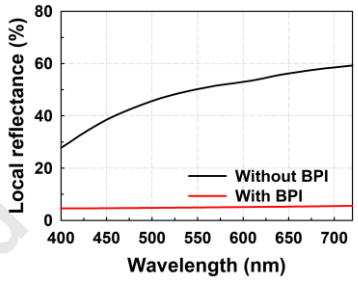

Fig. 3. Local reflectance of the Ag electrode region. Reflectance spectra without BPI (black line) and with BPI (red line), showing reduced local reflectance after BPI integration.

3.4. Characteristics of Metal Mesh Electrodes

The characteristics of the fabricated metal mesh electrodes were evaluated in terms of sheet resistance and optical transmittance. The mesh sheet resistance measured by the Van der Pauw method was 45.6 Ω/□, which is slightly higher than the theoretical value of 38.87 Ω/□ estimated from the mesh resistance model [23]. This difference can be attributed to practical variations introduced during fabrication, such as deviations in line width and mesh depth, as well as incomplete filling of the recessed channels with Ag NP ink. Nevertheless, the measured sheet resistance remained below the target value of $R_{s,mesh}$ < 50 Ω/□, indicating that the designed mesh geometry provided the intended electrical characteristics. In addition, the sheet resistance showed negligible change after the selective etching process, suggesting that removal of the exposed BPI regions did not significantly affect the Ag conductive network. The sheet resistance

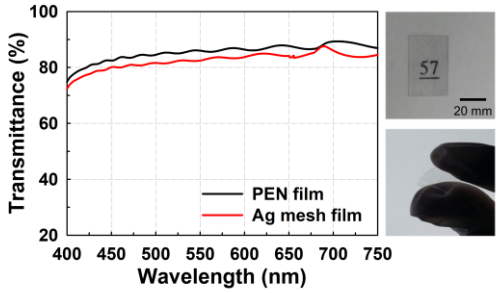

Fig. 4. Optical transmittance of the Ag metal mesh electrode film. Transmittance spectra of the bare PEN film and Ag metal mesh electrode film, with photographs showing the transparency and flexibility of the fabricated sample.

also showed negligible change after 1,000 bending cycles at a 30 mm bending radius.

The optical transmittance of the electrode film was measured using a UV–vis spectrophotometer in the wavelength range of 400–800 nm. At 550 nm, the bare PEN film exhibited a transmittance of 86.00%, whereas the metal mesh electrode film showed a transmittance of 81.92% (Fig. 4). Considering the transmittance of the PEN substrate, the normalized transmittance of the mesh structure was calculated to be approximately 95.25%, which agrees well with the design target of maintaining an open-area transmittance above 95%. The measured film transmittance was slightly lower than the theoretical value of 84.31%, likely due to residual particles or scattering centers remaining in the open regions after etching. Despite this slight optical loss, the fabricated electrode remained visibly transparent while meeting the target sheet resistance.

These results indicate that the fabricated electrode film satisfied the intended optical–electrical target range, while the main function of the localized BPI layer was to reduce reflection from the Ag mesh lines. The measured transmittance and sheet resistance should be interpreted together with the substrate and processing conditions used in this study, rather than as fixed limits of the proposed structure. Because the PEN substrate exhibited a transmittance of 86.00%, the total electrode-film transmittance was partly limited by the substrate, whereas the normalized transmittance of the mesh structure was approximately 95.25%. Therefore, the total transmittance could be further improved by using a substrate with higher intrinsic transparency. Similarly, the sheet resistance could be further reduced by optimizing the sintering conditions, using a higher-conductivity Ag NP ink, or increasing the mesh aspect ratio.

4. CONCLUSION

In this study, a flexible Ag metal mesh electrode integrated with a localized BPI light-absorption layer was shown to reduce metal-induced reflection. The carbon-black-dispersed PI layer was selectively retained beneath and near the Ag mesh region through thermal imprinting, Ag NP ink filling, thermal treatment, and selective etching, enabling local optical modification of the reflective metal-line region without coating the entire transparent electrode film with a light-absorbing layer. The localized BPI layer reduced the reflectance of the Ag electrode region from 50.22% to 4.94% at 550 nm, corresponding to a reduction of approximately 90.16%. Since the Ag mesh lines are the primary source of metal-induced reflection and pattern visibility, this local reduction in electrode-region reflectance offers a meaningful way to lower the apparent reflection of transparent metal mesh electrodes. The fabricated electrode satisfied the target mesh sheet resistance of $R_{s,mesh} < 50\ \Omega/\square$ and exhibited a transmittance of 81.92% at 550 nm. In addition, the sheet resistance showed negligible change after selective etching and repeated bending, suggesting that the localized BPI integration did not substantially disturb the Ag conductive network. These results suggest that integrating a localized light-absorption layer can be a useful design approach for low-reflectance, flexible metal-mesh TCEs while preserving their basic transparent-electrode characteristics.

ABBREVIATIONS

TCE: Transparent conducting electrode
ITO: Indium tin oxide
CNT: Carbon nanotube
BPI: Black polyimide
NP: Nanoparticle
PEN: Polyethylene naphthalate
PI: Polyimide
PDMS: Polydimethylsiloxane
UVO: Ultraviolet–ozone
OM: Optical microscopy

ACKNOWLEDGEMENTS

Author Contributions
JSP conducted the main experiments and analysis. JYJ contributed to experiments and discussion. JCC led the study and drafted the manuscript. HRK contributed to supervision and manuscript preparation. All authors read and approved the final manuscript.

Funding
This research was supported by the National Research Foundation of Korea (NRF) funded by the Korean government (MSIT) (No. RS-2024-00416272) and by the Technology Innovation Program (RS-2024-00453508, Development of technology to commercialize core optical components and modules for AR/MR devices to lead the XR optical components supply market) funded by the Ministry of Trade, Industry and Energy (MOTIE, Korea).

Declarations of Competing Interests
The authors declare that they have no competing interests.

REFERENCES

[1] Manchi, P.; Yoon, H.-J. Electrospun Nanofibers Based Flexible Triboelectric Nanogenerators for Mechanical Energy Harvesting and Smart Sensing Applications: A Review. Trans. Electr. Electron. Mater. 2026, 27(1), 90-99.

[2] Choi, J.-C.; Jeong, H. Y.; Sun, J.-H., Byun, J.; Oh, J.; Hwang, S. J. et al. Bidirectional Zero Poisson's Ratio Elastomers with Self-Deformable Soft Mechanical Metamaterials for Stretchable Displays. Adv. Funct. Mater. 2024, 34(52), 2406725.

[3] Kim, W.; Kwon, J.; Jung, S. 3D Integration of Flexible and Printed Electronics: Integrated Circuits, Memories, and Sensors. J. Flex. Print. Electron. 2023, 2(2), 199-210.

[4] Roy, A. B. Metal-Assisted Chemical Etching Based Microwell Structures for Thin and Flexible c-Si Solar Cell Application. Trans. Electr. Electron. Mater. 2025, 26(5), 765-773.

[5] Park, D. H.; Lee, D. W.; Jeong, H. Y.; Choi, J.-C.; Chung, S. Crosslinking Site Sharing-Driven Interface Engineering to Enhance Adhesion Between PDMS Substrates and Ag–PDMS Conductors. J. Mater. Chem. C. 2025, 13(41), 21137-21144.

[6] Yoo, C. J.; Yoon, J.; Kang, M.; Hong, Y. A Fully Embedded Stretchable Three-Dimensional Circuit via Highly Viscous Polydimethylsiloxane Bath. Trans. Electr. Electron. Mater. 2026, 27(3), 542-548.

[7] Yoo, H.; Lee, S.-H.; Kim, S.-M.; Jo, J.-H.; Kim, J.-Y. Research Progress in Flexible and Stretchable Encapsulation Materials for Electronics. J. Flex. Print. Electron. 2025, 4(1), 15-30.

[8] Park, D. H.; Lee, D. W.; Jeong, H. Y.; Choi, J.-C.; Chung, S. Auxetic Mechanical Metamaterials: Efficient Strain Engineering for Highly Reliable Free-Form Displays. J. Inf. Disp. 2025, 26(4), 447-460.

[9] Lee, S. J.; Lee, S. H.; Kang, H. W.; Nahm, S.; Kim, B. H.; Kim, H. et al. Flexible Electrochromic and Thermochromic Hybrid Smart Window Based on a Highly Durable ITO/graphene Transparent Electrode. Chem. Eng. J. 2021, 416, 129028.

[10] Im, H.-G.; Jang, J.; Jeon, Y.; Noh, J.; Jin, J.; Lee, J.-Y. et al. Flexible Transparent Crystalline-ITO/Ag Nanowire Hybrid Electrode with High Stability for Organic Optoelectronics. ACS Appl. Mater. Interfaces. 2020, 12(50), 56462-56469.

[11] Ellmer, K. Past Achievements and Future Challenges in the Development of Optically Transparent Electrodes. Nat. Photonics. 2012, 6(12), 809-817.

[12] Sharma, S.; Shriwastava, S.; Kumar, S.; Bhatt, K.; Tripathi, C. C. Alternative Transparent Conducting Electrode Materials for Flexible Optoelectronic Devices. Opto-Electron. Rev. 2018, 26(3), 223-235.

[13] Park, M.; Kang, S. H. Transparent Electrodes Using Solution-Processed Nanowires. J. Flex. Print. Electron. 2025, 4(2), 151-162.

[14] Kee, S.; Kim, N.; Park, B.; Kim, B. S.; Hong, S.; Lee, J.-H. et al. Highly Deformable and See-Through Polymer Light-emitting Diodes with All-Conducting-Polymer Electrodes. Adv. Mater. 2018, 30(3), 1703437.

[15] Jeon, I.; Yoon, J.; Kim, U.; Lee, C.; Xiang, R.; Shawky, A. et al. High-Performance Solution-Processed Double-Walled Carbon Nanotube Transparent Electrode for Perovskite Solar Cells. Adv. Energy Mater. 2019, 9(27), 1901204.

[16] Lu, X.; Zhang, Y.; Zheng, Z. Metal-Based Flexible Transparent Electrodes: Challenges and Recent Advances. Adv. Electron. Mater. 2021, 7(5), 2001121.

[17] Althumayri, M.; Das, R.; Banavath, R.; Beker, L.; Achim, A. M.; Koydemir H. C. Recent Advances in Transparent Electrodes and Their Multimodal Sensing Applications. Adv. Sci. 2024, 11(38), 2405099.

[18] Kim, D.; Jeong, S.; Lee, D. K.; Yi, W.; Yoon, H.; Jeon, J. et al. High-Performance Transparent Metal Mesh Electrodes Utilizing a Metal-Vapor-Desorption Layer for Organic Light-Emitting Diode Applications. Mater. Horizons. 2026, 13(10), 4863-4874.

[19] Yoon, S. J.; Min, J.; Ko, S. H. Fabrication of Flexible Printed Electronic Using Selective Laser Sintering. J. Flex. Print. Electron.

2022, 1(2), 189-199.

[20] Li, Z.; Li, H.; Zhu, X.; Peng, Z.; Zhang, G.; Yang, J. et al. Directly Printed Embedded Metal Mesh for Flexible Transparent Electrode via Liquid Substrate Electric-Field-Driven Jet. Adv. Sci. 2022, 9(14), 2105331.

[21] Fernandes, I. J.; Aroche, A. F.; Schuck, A.; Lamberty, P.; Peter, C. R.; Hasenkamp, W. et al. Silver Nanoparticle Conductive Inks: Synthesis, Characterization, and Fabrication of Inkjet-Printed Flexible Electrodes. Sci. Rep. 2020, 10(1), 8878.

[22] Park, J.-S.; Choi, J.-C.; Park, M.-K.; Bae, J. M.; Bae, J.-H.; Kim, H.-R. Microtransfer Printing of Metal Ink Patterns onto Plastic Substrates Utilizing an Adhesion-Controlled Polymeric Donor Layer. J. Micromech. Microeng. 2016, 26(6), 065008.

[23] Ghosh, D. S.; Chen, T. L.; Pruneri, V. High Figure-of-Merit Ultrathin Metal Transparent Electrodes Incorporating a Conductive Grid. Appl. Phys. Lett. 2010, 96(4), 041109.